Birhanu, Y., Wilks, M., Biggs, J., Kendall, J. M., Ayele, A., & Lewi, E. (2018). Seasonal patterns of seismicity and deformation at the Alutu geothermal reservoir, Ethiopia, induced by hydrological loading. *Journal of Volcanology and Geothermal Research*. https://doi.org/10.1016/j.jvolgeores.2018.03.008
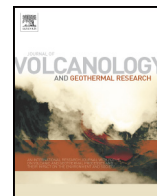
University of Bristol - Explore Bristol Research
General rights

Seasonal patterns of seismicity and deformation at the Alutu geothermal reservoir, Ethiopia, induced by hydrological loading

Yelebe Birhanu [a], Matthew Wilks [a,b], Juliet Biggs [a,*], J-Michael Kendall [a], Atalay Ayele [c], Elias Lewi [c]

[a] *School of Earth Sciences, University of Bristol, Queens Road, Bristol BS8 1RJ, United Kingdom*
[b] *Norsar, Gunner Randers vei 15, Kjeller 2007, Norway*
[c] *Institute of Geophysics, Space Science and Astronomy, Addis Ababa University, Addis Ababa, Ethiopia*

ARTICLE INFO

ABSTRACT

Seasonal variations in the seismicity of volcanic and geothermal reservoirs are usually attributed to the hydrological cycle. Here, we focus on the Aluto-Langano geothermal system, Ethiopia, where the climate is monsoonal and there is abundant shallow seismicity. We deployed temporary networks of seismometers and GPS receivers to understand the drivers of unrest. First, we show that a statistically significant peak in seismicity occurred 2–3 months after the main rainy season, with a second, smaller peak of variable timing. Seasonal seismicity is commonly attributed to variations in either surface loading or reservoir pore pressure. As loading will cause subsidence and overpressure will cause uplift, comparing seismicity rates with continuous GPS, enables us to distinguish between mechanisms. At Aluto, the major peak in seismicity is coincident with the high stand of nearby lakes and maximum subsidence, indicating that it is driven by surface loading. The magnitude of loading is insufficient to trigger widespread crustal seismicity but the geothermal reservoir at Aluto is likely sensitive to small perturbations in the stress field. Thus we demonstrate that monsoonal loading can produce seismicity in geothermal reservoirs, and the likelihood of both triggered and induced seismicity varies seasonally.

© 2018 Published by Elsevier B.V.

1. Introduction

Induced or triggered seismicity can be caused by transient changes in reservoir stress conditions. Induced seismicity is associated with anthropogenic fluid injection at geothermal and hydrocarbon reservoirs (e.g. Ellsworth, 2013; Gaucher et al., 2015; Grünthal, 2014; Verdon, 2014), or surface loading such as water impoundment (e.g. Simpson et al., 1988; Talwani et al., 2007). Natural processes, such as ice sheet unloading (e.g. Stewart et al., 2000), dynamic stresses from large, distant earthquakes (e.g. Prejean et al., 2004), or magmatic overpressure (e.g. Ebmeier et al., 2016) can also trigger seismicity in critically stress reservoirs.

Seasonal variations in the number of small (M < 4) and shallow (<5 km) seismic events have been observed at a range of settings including, at volcanoes (e.g. Christiansen et al., 2005; Saar and Manga, 2003; Wolf et al., 1997), faults (Bettinelli et al., 2008; Christiansen et al., 2007; Hainzl et al., 2006) and intraplate settings (Costain and Bollinger, 2010; Costain et al., 1987). Two hydrological mechanisms have been proposed to account for these observations 1) loading due to seasonal changes in surface and near-surface water storage, and 2) increased pore-pressure along faults within the reservoir due to

subsurface recharge (Saar and Manga, 2003). The time delay between peak surface runoff and peak seismicity varies from days to months and is attributed to the timescale of groundwater recharge, governed by pore-fluid pressure diffusion (Hainzl et al., 2006; Lee and Wolf, 1998; Saar and Manga, 2003).

Hydrological processes also cause seasonal patterns in vertical displacements and these can be measured by the Global Positioning System (GPS). GPS-derived estimates of ground-water storage correspond well with those made by the Gravity Recovery and Climate Experiment (GRACE) (Fu et al., 2015). Surface loading causes subsidence, with snowfall causing an instantaneous elastic response (Argus et al., 2014) and monsoonal loading causes delayed subsidence with the delay attributed to the timescale of ground-water recharge (Birhanu and Bendick, 2015). In contrast, fluid injection into reservoirs is typically associated with uplift (Vasco et al., 2010; Vasco et al., 2013) and extraction with subsidence (Fialko and Simons, 2000; Parker et al., 2017).

In this paper, we use a network of continuous GPS (cGPS) and seismometers at Aluto-Langano geothermal reservoir, Ethiopia to study seasonal patterns of deformation and seismicity. Aluto volcano is known to be actively deforming and experiences a monsoonal climate, while the geothermal system generates significant seismicity. In theory, increased loading due to lake level rise will cause subsidence, while increased pore pressure within the reservoir would cause uplift. Thus we

investigate the relationship between seismicity, deformation, precipitation and lake level to better understand the stress state of geothermal reservoirs.

2. Background

The Aluto-Langano system lies in the Main Ethiopian Rift, between Lake Ziway to the north and Lake Langano to the south (Fig. 1). The Main Ethiopian Rift divides the Nubian and Somalian plates at a rate of ~5–6 mm/year (Bendick et al., 2006; Bilham et al., 1999). Magmatic segments in the rift floor accommodated ~80% of the strain (Birhanu et al., 2016; Kogan et al., 2012) and most of the seismicity (Ayele and Kulhánek, 1997; Keir et al., 2006; Mazzarini et al., 2013). At Aluto, large ignimbrite forming eruptions took place at ~316 ka and 306 ka (Hutchison et al., 2016c), with post-caldera, edifice building volcanism consisting of highly-evolved peralkaline rhyolite lavas, ignimbrites and pumice fall deposits starting at ~55 ka (Hutchison et al., 2016a). The most recent eruption has been dated at ~400 years ago (Hutchison et al., 2016a). Magnetotelluric studies show a highly conductive clay cap in the upper 2 km, but no evidence for a deeper magmatic system (Samrock et al., 2015).

A two-year seismic deployment detected 1361 earthquakes in a 15 km radius area around Aluto, ranging in magnitude from −0.4 to 3.0 (Wilks et al., 2017). The majority of events (760 of 1361) were located within the geothermal reservoir (Fig. 2), defined as 1) 2 km from the surface (above sea level), and b) within 15 km from the centre of the caldera (defined as seismic station A01E). Applying a Gutenberg-Richter relationship to this subset, gives a b-value of 2.55 ± 0.55 and high seismicity rate (a = 5.64), consistent with other volcanic environments where circulation of fluids means strain is preferentially released by numerous small events (Wilks et al., 2017). Fault plane solutions for

a subset of the deeper and off-edifice events show ~NNE-SSW normal faults, consistent with the current direction of extension. No fault plane solutions are available for the shallow events.

Surface deformation measurements from satellite InSAR have shown two pulses of uplift in 2004 and 2008 (>15 cm) separated by periods of slow (~3 mm/year) subsidence (Biggs et al., 2011; Hutchison et al., 2016b). It is not possible to discriminate between magmatic and hydrothermal processes using deformation alone, but the uplift episodes at Aluto are interpreted to represent the repeated injection of magmatic fluids to shallow (<5 km) depths causing inflation, whereas the cooling and flow of hydrothermal fluids causes the subsequent subsidence (Hutchison et al., 2016b).

Pathways for fluids are controlled by shallow structures including the NNE-SSW Artu Jawe Fault Zone (AJFZ) which crosscuts the volcanic edifice and a caldera ring fault (Braddock et al., 2017; Hutchison et al., 2015). The majority of geothermal fluids are derived from precipitation on the rift flanks, with <10% from nearby lakes (mainly from lake Ziway) (Darling et al., 1996). Although there is no long-term ground-based monitoring, the distribution and the fumaroles can be mapped using a 12 year archive of thermal infrared images from the ASTER satellite. The temperature and extent of the fumaroles show no relation to the surface deformation, but the Bobesa fumaroles, located along the caldera ring fault in the east, show a delayed response to rainfall (Braddock et al., 2017). Geothermal development at Aluto-Langano began in 1981 (Hochstein et al., 2017) and continue at the present time. The plant was only operational for a small fraction of the experiment (14th January 2012 until 4th July 2012) with power production ranging from 10-35MWh during this period.

Lake Ziway is the largest volume fresh water lake in the Main Ethiopian Rift with surface area 440 km^2 and maximum depth of 8.9 m and is the only source of fresh water to the town of Ziway and nearby villages
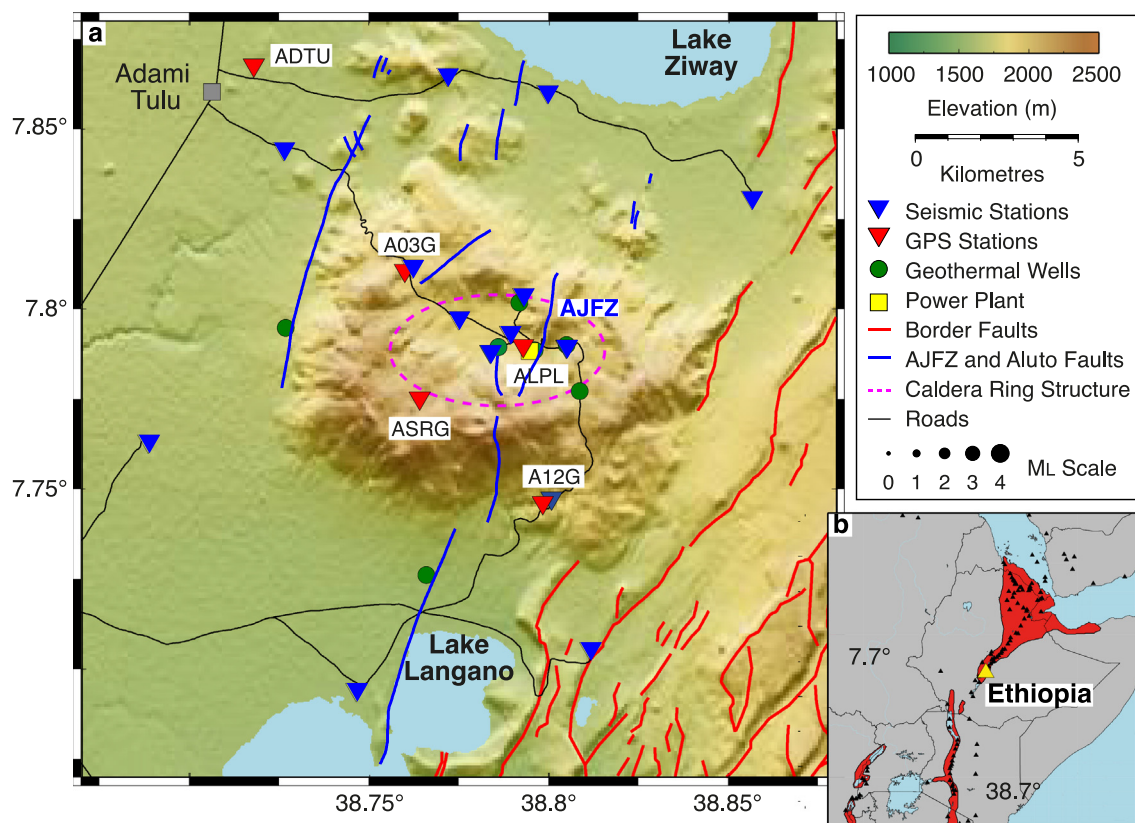
Fig. 1. a) Topographic map of Aluto volcano showing the seismic and GPS network, the Aluto-Langano Geothermal Power Plant and geothermal wells. Border faults are red (Agostini et al., 2011) while the Artu Jawa fault zone (AJFZ) and other faults of the Aluto volcanic complex are blue (Kebede et al., 1985; Hutchison et al., 2015). b) Location of Aluto volcano. (For interpretation of the references to colour in this figure legend, the reader is referred to the web version of this article.) Modified from Wilks et al. (2017).
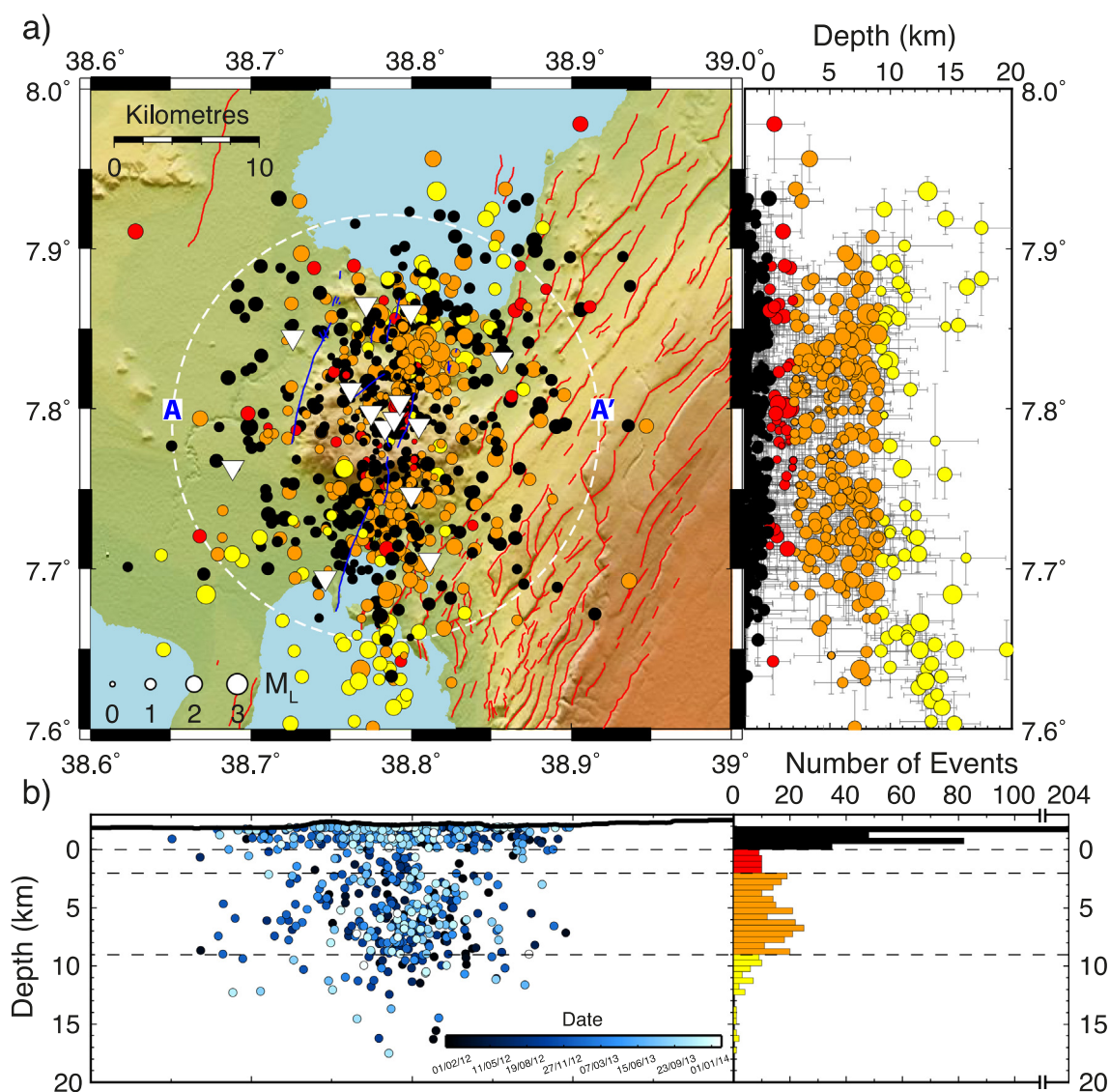
Fig. 2. Seismicity at Aluto-Langano volcano. a) Earthquake locations in 2012–2014 recorded by the ARGOS network (Wilks et al., 2017). Basemap as for Fig. 1. White triangles are the seismometer locations, the event size is denoted by circle size and depth by colour (Wilks et al., 2017). b) Earthquake catalogue projected onto an E-W profile, with event date denoted by colour. The histogram shows that the majority of events occur within the upper 2 km (above sea level), which corresponds to the geothermal reservoir. (For interpretation of the references to colour in this figure legend, the reader is referred to the web version of this article.)
Modified from Wilks et al. (2017).

(Ayenew, 1998). Lake Langano is smaller in area (230 km^2), but deeper, with a maximum depth of 46 m. High sulphur levels mean it is brown in colour, and the lake is mostly used for recreational purpose by tourists and villagers (Mepham et al., 1992). The two lakes have different elevations (Lake Ziway at 1636 m and Lake Langano at 1582 m above sea level) and fluid flow from north to south occurs through groundwater flow and along the Bulbula River (Mepham et al., 1992).

Precipitation is bimodal with one short rainy season from February to May (monthly average < 150 mm), known locally as Belg, and a long and heavy rainy season from June to September (monthly average > 150 mm), known locally as Kiremt. Although the intensity of precipitation varies from year to year, this pattern remains consistent.

3. Methods

We use data from twelve seismometers, four cGPS stations, monthly precipitation and lake level records to study the seasonal variations of

seismicity at Aluto-Langano hydrothermal and magmatic systems (Figs. 3, 4).

3.1. Seismicity

A temporary network of seismometers was installed at Aluto volcano between January 2012 and January 2014 and the spatial pattern of seismicity has been described by (Wilks et al., 2017). We use the same event catalogue and explore the temporal characteristics of the seismicity, before comparing the results to deformation measurements. We briefly summarize the deployment and location methods but refer to (Wilks et al., 2017) for further details. The network consisted of 12 three-component broadband stations located within and around the caldera, providing good spatial coverage (Fig. 1). For accurate event location, we use the nonlinear global-search earthquake location tool, NONLINLOC (Lomax et al., 2000) and a 1D velocity model combining data from regional tomography and local well-log data as described in (Wilks et al., 2017). In the uppermost 2–3 km, lithologies determined
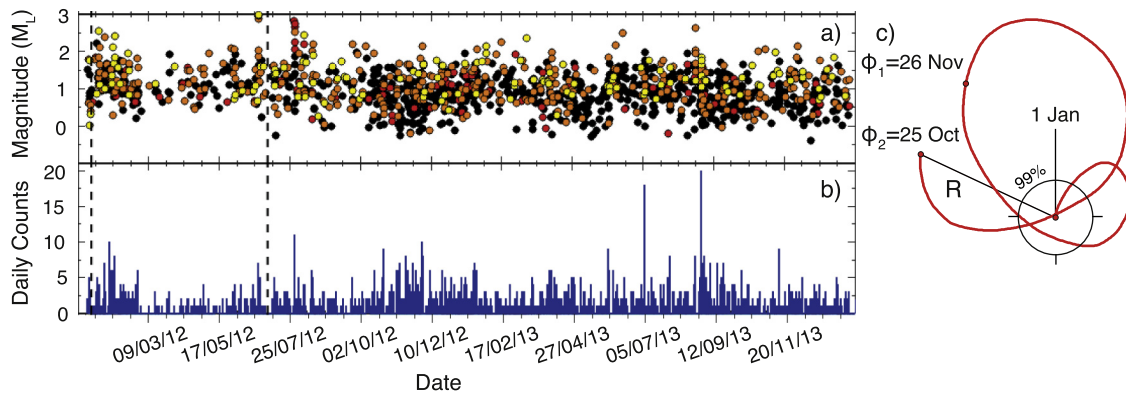
Fig. 3. Temporal Variation in seismicity within the geothermal reservoir at Aluto-Langano volcano. a) seismic moment, b) daily earthquake count, c) Schuster diagram showing seasonality. Shallow seismicity includes 760 events from a 2 year period at depths <2 km and within a 15 km radius of the caldera centre. The days on which earthquakes occur are converted to vectors and summed, such that the position after a year corresponds the peak of seismicity. The poles at time zero and after one and two years are the red circles. The concentric circles represent confidence intervals of 95% and 99% respectively that the seismicity does not satisfy the null hypothesis of a uniform distribution. The resultant vector has the pole, $\varphi = 295.3°$ and length, $R = 113.9$. (For interpretation of the references to colour in this figure legend, the reader is referred to the web version of this article.)

from well-log data (Gianelli and Teklemariam, 1993; Gizaw, 1993; Teklemariam et al., 1996) were mapped to seismic velocities (Christensen, 1984; Press, 1966). At greater depths the velocity structure is taken from a passive-source tomographic study (Daly et al., 2008).

We focus our analysis on the subset of 760 events within 15 km of the caldera and in the upper 2 km, which represents the geothermal reservoir. We test for seasonality in the seismicity by discounting the null hypothesis that events are distributed as a random Poisson process throughout the year (Schuster, 1898). Known as a Schuster test, this is done by converting each day of earthquake occurrence to a polar vector of unit length and a phase angle (ω) from 1 to 360° (1st January = 0°) and then vectorially adding over the number of events (N) (Fig. 3). If this vector, $R = \sqrt{A^2 + B^2}$ where $A = \sum_{i=1}^{N} \cos\omega_i$ and $B = \sum_{i=1}^{N} \sin\omega_i$, exceeds a certain length then the null-hypothesis of a completely random distribution can be rejected and it can be concluded that the tendency of earthquakes to occur around the date indicated by the resultant vector is statistically significant (e.g. Jiménez and García-Fernández, 2000; McClellan, 1984). We also tested for clustering using a range of algorithms (Gardner and Knopoff, 1974; Reasenberg, 1985; Uhrhammer, 1986). We then apply a moving average of 30 days for

comparison to the monthly cGPS displacement time series, precipitation and lake level datasets (Section 5.2).

3.2. GPS

Continuous GPS sites at Aluto volcano were installed in early 2013 in order to study the temporal and spatial variation of deformation related to the hydrothermal and magmatic processes. We use data from the period March 2013–December 2015, with data recorded at a 30 s sampling interval. Finding secure and stable locations for the sites was challenging. Most houses, schools and clinics in the region are constructed of wood and mud and situated on flat-lying lands comprised of old lake sediments or volcanic deposits. The volcanic edifice is comprised of obsidian flows typically <10 m thick, interbedded with volcaniclastic deposits. We chose to locate our sites on major obsidian flows, close to houses for security reasons. For all sites, a local person was contracted as a guard, and where appropriate, a thorn bush fence was built around the site to deter animals. The gaps in time series (Fig. 4) reflect the difficulty in operating and maintaining GPS equipment in areas such as this, which are further compounded by the necessity for short-term funding and equipment loans.
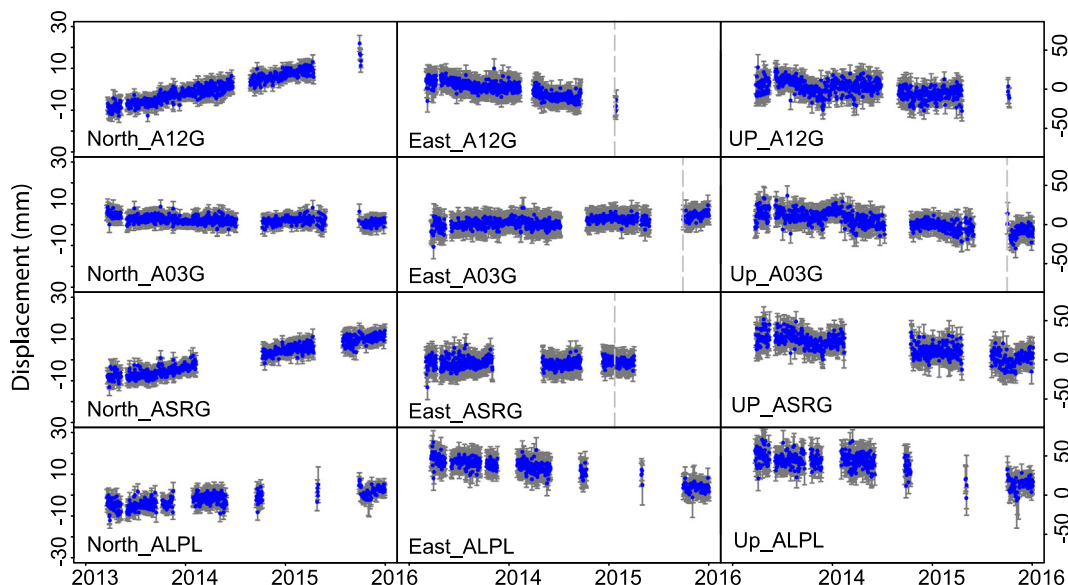
Fig. 4. Daily time series of continuous GPS measurements at Aluto-Langano volcano, Ethiopia. Location of GPS sites is given in Fig. 1.

Four cGPS sites are located on the volcanic edifice (ASRG, A03G, A12G, ALPL). The reference site (ADTU) is on the roof of a house in the Ethiopian Electrical Power Corporation (EEPCO) compound in Adami Tulu located ~15 km away from the volcano (Fig. 1). The design of the building was altered to provide a solid platform; the breeze blocks above the major structural beam were filled with cement and the antenna mast drilled directly into that. ASRG is located in the SW part of the caldera and is the highest elevation station at 2133 masl (Fig. 2). A03G is located at the NW part of the caldera at an elevation of 1975 masl overlooking lake Ziway (Fig. 2). A12G is located on the southern rim of the caldera, close to Lake Langano (~5 km) at an elevation of 1851 masl. The site was abandoned in July 2015 due to security issues, and after this date, only campaign measurements are available. ALPL is located at the centre of the caldera (Fig. 2) and close to the AJFZ which is the primary pathway for hydrothermal upwelling (Hutchison et al., 2015). The station is mounted on the roof of a service building associated with the geothermal power station, but the power plant was mostly non- operational during this time period and is not thought to have affected the measurements.

The coordinates of the cGPS sites were processed using the GAMIT/GLOBK software developed by MIT (Herring et al., 2010) with corrections for the ionosphere and modeled wet troposphere (Reilinger et al., 2006). We used 12 IGS reference sites including ADIS station, which is located ~130 km from Aluto to generate the daily solutions in the International Terrestrial Reference Frame 2014 (ITRF14) (Altamimi et al., 2016). Daily position solutions were then corrected for ocean loading using the FES2004 model and the wet zenith delay using standard hydrostatic model in GAMIT (Herring et al., 2010). The daily solutions (h-files) were then combined with the daily global solutions (H-files) obtained from MIT, using the global Kalman filter in GLOBK. We then inspect the position of the north, east and vertical coordinates in order to remove outliers above two-sigma uncertainties and offsets caused by antenna change, earthquakes, and any other phenomena (Fig. 4). As Aluto is known to be subsiding (Biggs et al., 2011), we remove a linear trend using a weighted least squares approach. The de-trended daily positions were then aggregated into weekly and monthly time series (Fig. 5c).

3.3. Precipitation and lake level

We use monthly average precipitation data from the Climate Research Unit (CRU) database (Harris et al., 2014), which is processed monthly and has spatial resolution of $0.5° × 0.5°$. The lake level data for Lake Ziway was collected by Ziway Fisheries Research Center (Senbete, 2014). Lakes Abijata, Langano and Shala lie to the south of Aluto and likely contribute to the lake loading, but the level of the lakes is not monitored.

4. Results

4.1. Surface deformation

Fig. 5 shows the comparison between monthly time-series of vertical deformation, lake level and precipitation. In 2014, precipitation followed a typical bimodal pattern with ~10 cm during the light rains in May and a more intense, and longer rainy season, peaking at ~19 cm in September. In 2013, the rains were unusually continuous with peaks of precipitation of ~25 cm in May and ~19 cm in August. The lake level has a single broad maximum in September–November and is lowest around May. The peak occurs ~1–2 months after the heavy rains, and the time lag can be attributed to the time taken for recharge of the lakes by tributaries which drain water from the Ethiopian Plateau. The light rains in May appear to have little impact on the lake level.

At sites A12G, A03G and ARSG, located on the caldera rim, the vertical component of each cGPS displacement time series show seasonal
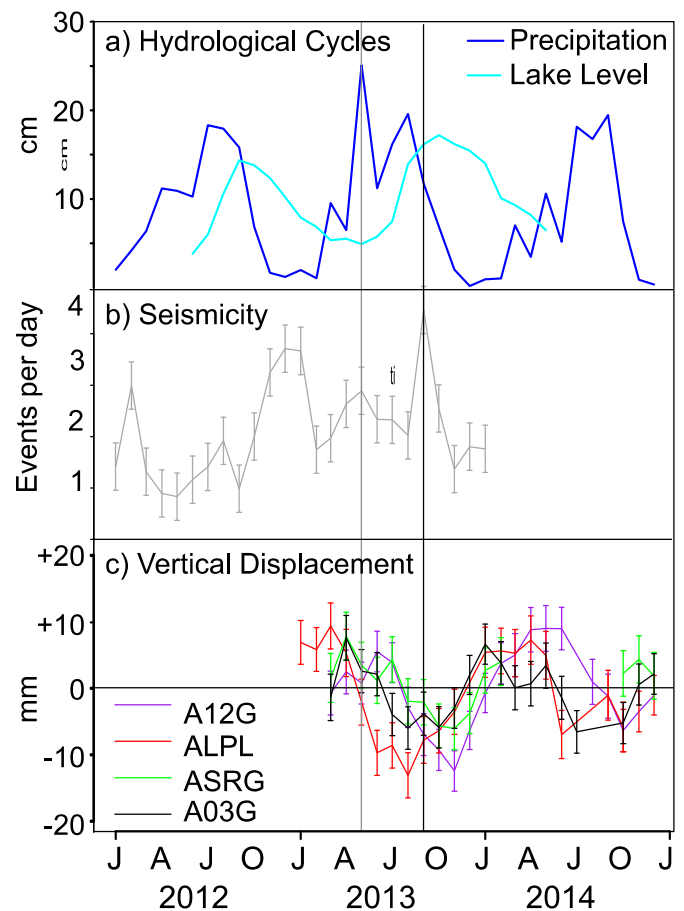
Fig. 5. Monthly time series of precipitation, lake level, seismicity and vertical deformation at Aluto-Langano volcano, Ethiopia. a) Hydrological cycles. Precipitation data is from the Climate Research Unit (Harris et al., 2014) and lake level of Lake Ziway from the Ziway Fisheries unit (Senbete, 2014). b) Seismicity. Based on a monthly average from a network of 12 seismometers. c) Vertical displacement from four cGPS sites (ALPL, ASRG, A12G and A03G), which have been detrended to remove ongoing subsidence. Vertical black line shows the primary peak of seismicity in 2013 and the grey line shows the secondary peak.

variations of ~±10 mm, above error. Peak subsidence occurs 2–3 months after the peak of precipitation, consistent with measurements at cGPS sites elsewhere in Ethiopia (Birhanu and Bendick, 2015) and coincident with the maximum lake level. There is a single broad peak of subsidence, similar to the lake level curve but unlike the bimodal pattern of precipitation, thus further supporting the suggestion that the subsidence is an elastic response to the surface load. The north-south and east-west components show no annual variability above the uncertainty (~2 mm), consistent with a loading model for which the vertical component would be several times larger than the horizontal component (Wahr et al., 2013). As there is no long-term geophysical monitoring at Aluto, our analysis relies on temporary deployments, which have insufficient overlap to statistically test the correlations between datasets.

The time-lag at site ALPL is much shorter than at the other sites, with the maximum subsidence occurring during the rainy season itself. The annual signal is greatest in the vertical component (~20 mm) but also appears at a lower magnitude in the north-south (3 mm) and east-west (3 mm) components. The explanation for this anomalous behavior may lie in the location of ALPL, which sits on the caldera floor, close to the Artu Jawe Fault zone and the geothermal plant. Firstly, there is transient local loading associated with a shallow lake that forms during heavy rainfall, and disperses again within weeks. The time taken for water to drain from the caldera rim into the central caldera is much shorter than from the plateau into the lakes, thus the time lag is much

shorter. More significantly, the Artu Jawe Fault zone is a major pathway for hot upwelling fluids, which may also facilitate downwards flow of cold meteoric water. Although Braddock et al. (2017) showed that the fumaroles along the Artu Jawe Fault zone did not have a seasonal response to precipitation, the structure may still reduce the time taken to recharge shallow ground-water aquifers.

4.2. Seismicity

Applying the Schuster test to the selected subset of 760 earthquakes occurring over a duration, $t = 752$ days, produce a resultant vector pole, $\varphi = \tan^{-1}(B/A)$ at an angle of ~295°, which corresponds to 25th October (Fig. 3). With just two years of data, there is uncertainty in the calculation of the pole, which is illustrated by the difference between the angle of the resultant vector following one year (26th November) and after two years (25th October).

The probability P (P-value), of a random walk being equal to or greater than distance R is given by $P = e^{-R^2/N}$ ($N \geq 10$), where the lower the P-value, the higher the probability that the stacked distribution over the period is non-random. Although two years is a relatively short period of time to perform a Schuster test, the vector length, $R = 112$, corresponds to a P-value of 3.86×10^{-8} which exceeds the 99% confidence limit for all periods, $T \geq 1$ day ($P = 1.33 \times 10^{-5}$ (Ader and Avouac, 2013)). This indicates that the temporal distribution of these shallow events contains a non-random component.

The declustering algorithms (Gardner and Knopoff, 1974; Reasenberg, 1985; Uhrhammer, 1986) did not detect any statistically significant aftershocks, likely because the background seismicity has a high b-value, and few large events occurred. Visual inspection corroborates that the largest magnitude events, such as the M > 2.5 in 2012, are not followed by a significant number of aftershocks and this is not the cause of the non-random behavior.

The peak in seismicity corresponds to highs of both lake level and subsidence, which implies that the seismicity is caused by an increase in surface load. The precise timing of the peak depends on the timing of the peak rainfall, which varies from year to year. In addition to the major peak in October/November of identified by the Schuster analysis, there are secondary peaks in August 2012 and May 2013. These secondary peaks have 1.5–2.5 events per day compared to an average of 3–4 events per day for the major peak and may not be statistically significant. This secondary peak occurred towards the end of the main rainy season in 2012 and towards the start in 2013. During 2013, when both GPS and seismometers were deployed, the secondary peak in seismicity corresponds to a period of uplift, which is consistent with the hypothesis that the secondary peak in seismicity is caused by recharge of the subsurface hydrothermal reservoir. However, due to the low amplitude and variable timing, the existence and mechanism of this minor peak in seismicity remains ambiguous.

5. Discussion

5.1. Timescale and mechanism of reservoir response

We use Mohr circles to illustrate the principles behind the two proposed mechanisms of seasonal seismicity, surface loading and reservoir overpressure (Fig. 6). An increase in surface and near-surface loading increases vertical stress, which in a rift setting is the largest principal stress, σ_1, and increases the size of the Mohr circle (Fig. 6a). An increase in reservoir pore-pressure, p_f, will decrease the effective normal stress, $\sigma_n' = \sigma_n - p_f$, moving the Mohr circle to the left (Fig. 6b). The consequence of both mechanisms is that the stress envelope intersects the Coulomb failure criteria, $\tau = \tau_0 + \mu \sigma_n'$ triggering seismicity, where μ is the effective coefficient of friction.

Seasonal seismicity has also been documented in the Canary Islands, where the rainfall and seismicity are contemporaneous (Jiménez and
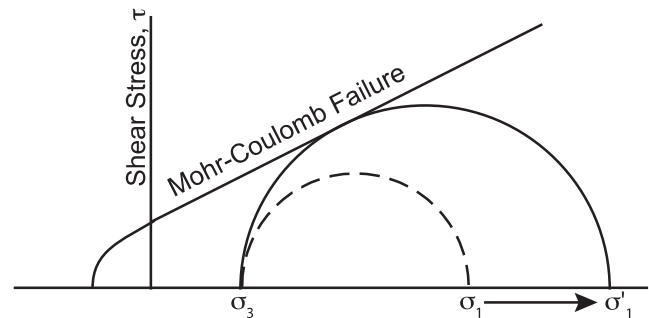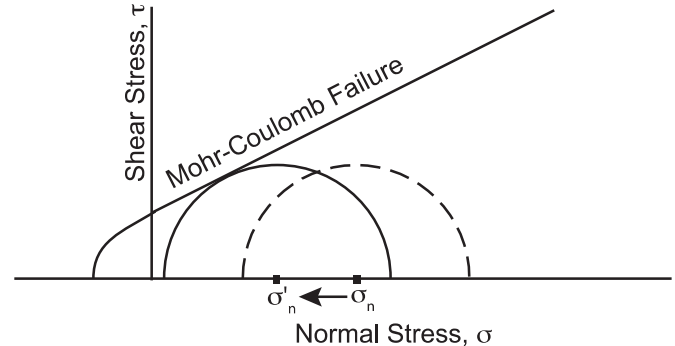
Fig. 6. Proposed mechanisms of seasonal seismicity, illustrated using Mohr circles. The dashed semi-circle is the initial stress state and the solid semi-circle the final stress state. (a) An increase in surface loading, increases σ_1, causing the Mohr circle to expand and intersect the Coulomb failure criteria, $\tau = \tau_0 + \mu \sigma_n'$ where μ is the effective coefficient of friction. (b) An increase in pore-fluid pressure, p_f decreases the effective normal stress, $\sigma_n' = \sigma_n - p_f$, on the fault, causing the Mohr circle to shift to the left, and intersect the Coulomb failure criteria.
(After Saar and Manga (2003).)

García-Fernández, 2000), and at Mt Hood in the Cascades where the delay between precipitation and seismicity is on the order of 5 months, and is driven by an increase in reservoir pore pressure (Saar and Manga, 2003). In contrast, our observations at Aluto suggest that the primary peak in seismicity is contemporaneous with the maximum lake loading and associated with subsidence.

The mechanism and timescale of response for a given reservoir is dependent on reservoir geometry, fluid pathways and material properties. At Mt Hood, the seismicity occurs at ~4.5 km and the delay is consistent with the time needed for diffusion over this distance (Saar and Manga, 2003). At Aluto, we only consider seismicity at depths < 2 km, and the downward flow of cold, meteoric water may be enhanced by edifice-crossing faults, which are known to act as permeable pathways for upwelling hydrothermal fluids and gases (Braddock et al., 2017; Hutchison et al., 2015).

Similarly, the magnitude of the annual cycle of surface loading will depend on local variations in hydrology and climate. Ethiopia's monsoonal climate drives large seasonal variations in lake and water-table levels, and the topography of the rift causing a significant time delay between rainfall on the rift flank and filling of the lakes. Large seasonal variations in seismicity rates might also be expected at snow-capped volcanoes whereas in temperate climates, seasonal variations in loading may be insufficient to cause a measurable change in seismicity.

5.2. Loading stress

A stress change on the order of ~0.1 MPa is typically considered necessary to trigger seismicity, particularly when considering aftershocks (e.g. Beeler and Lockner, 2003). The seasonal stress imposed at Aluto-Langano will have contributions from both surface (lake) and

subsurface (vadose zone) components and can be estimated from GRACE satellite data, which measured the large-scale variation in water storage. For the central Main Ethiopian Rift, the annual variability in liquid water equivalent thickness was found to be ~6 cm (Birhanu and Bendick, 2015; Landerer and Swenson, 2012), equivalent to a vertical load of <1 kPa. Although this is sufficient to produce seasonal vertical deformation of up to 10 mm at GPS sites in the region (Birhanu and Bendick, 2015), it would be unlikely to trigger regional seismicity.

The heterogeneous distribution of surface and subsurface water storage, means the 1° resolution of the GRACE satellite is unlikely to capture the spatially variability in the magnitude of surface loading. For example, the 10–15 cm variation in height of Lake Ziway is twice that inferred from the GRACE measurements. Although monitoring data is not available for Lakes Abijata, Langano and Shala, we expect the variations in lake level to be larger there as the wide, shallow Lake Ziway produces a more muted response to hydrological changes than its neighbours. For example, studies have shown that water abstraction projects in the Lake Ziway catchment caused a greater longer-term reduction in the Lake Abijata water level than for Lake Ziway (Ayenew and Legesse, 2007). However, even taking the local variations into account, the magnitude of the loading is likely to be <0.01 MPa, below the threshold typically considered for aftershocks or regional earthquakes (0.1 MPa).

The response to loading is restricted to shallow seismicity occurring within Aluto's geothermal reservoir with no seasonal pattern in regional or deep seismicity. Hydrothermal systems, particularly those containing gas bubbles, are more sensitive to small stress changes than surrounding areas. Distant large earthquakes have caused seismic swarms (e.g. Prejean et al., 2004) and subsidence (Pritchard et al., 2013) at hydrothermal systems in response to dynamic stresses as low as 0.01 MPa. The abundant seismicity, high b-value (Wilks et al., 2017) and low V_p/V_s ratio of the Aluto geothermal reservoir suggest it is gas-rich and critically-stressed, thus sensitive to small-magnitude seasonal variations in stress associated with hydrological loading. Alternatively, stress changes can cause failure of an impermeable barrier, causing brecciation of a shallow aquifer and inducing seismicity (De Natale et al., 2001).

6. Conclusion

Seasonal variations in seismicity are seen across a range of settings, including in hydrothermal reservoirs. We combine observations of seismicity at Aluto volcano, Ethiopia, with geodetic measurements from a GPS network and hydrological observations to distinguish between possible mechanisms for seasonal seismicity. We conclude that the major seasonal peak in seismicity is driven by an increase in vertical loading as the lakes and groundwater aquifers fill. The magnitude of the stress change is insufficient to cause a regional change in crustal seismicity, but the Aluto-Langano geothermal reservoir is gas-rich and critically-stresses, thus particularly sensitive to low magnitude stress changes. Thus seismic and GPS data suggests that fractured reservoirs are closer to failure during at times of the year defined by the local hydrology, reservoir geometry and fluid pathways.

Key points

- Seasonal variations in seismicity occur in the geothermal field at Aluto, Ethiopia, indicating the reservoir is critically stressed.
- The peak in seismicity is driven by surface loading, as it is coincident with high lake.

Acknowledgements

References

Ader, T.J., Avouac, J.-P., 2013. Detecting periodicities and declustering in earthquake catalogs using the Schuster spectrum, application to Himalayan seismicity. Earth Planet. Sci. Lett. 377, 97–105.

Agostini, A., Bonini, M., Corti, G., Sani, F., Manetti, P., 2011. Distribution of quaternary deformation in the central Main Ethiopian Rift, East Africa. Tectonics 30 (4).

Altamimi, Z., Rebischung, P., Métivier, L., Collilieux, X., 2016. ITRF2014: a new release of the International Terrestrial Reference Frame modeling nonlinear station motions. J. Geophys. Res. Solid Earth 121 (8), 6109–6131.

Argus, D.F., Fu, Y., Landerer, F.W., 2014. Seasonal variation in total water storage in California inferred from GPS observations of vertical land motion. Geophys. Res. Lett. 41 (6), 1971–1980.

Ayele, A., Kulhánek, O., 1997. Spatial and temporal variations of seismicity in the Horn of Africa from 1960 to 1993. Geophys. J. Int. 130 (3), 805–810.

Ayenew, T., 1998. The Hydrogeological System of the Lake District Basin, Central Main Ethiopian Rift. Free University of Amsterdam, The Netherlands, p. 259 (Published PhD thesis, ISBN 9061641586).

Ayenew, T., Legesse, D., 2007. The changing face of the Ethiopian rift lakes and their environs: call of the time. Lakes Reserv. Res. Manag. 12 (3), 149–165.

Beeler, N., Lockner, D., 2003. Why earthquakes correlate weakly with the solid Earth tides: effects of periodic stress on the rate and probability of earthquake occurrence. J. Geophys. Res. Solid Earth 108 (B8).

Bendick, R., McClusky, S., Bilham, R., Asfaw, L., Klemperer, S., 2006. Distributed Nubia–Somalia relative motion and dike intrusion in the Main Ethiopian Rift. Geophys. J. Int. 165 (1), 303–310.

Bettinelli, P., Avouac, J.-P., Flouzat, M., Bollinger, L., Ramillien, G., Rajaure, S., Sapkota, S., 2008. Seasonal variations of seismicity and geodetic strain in the Himalaya induced by surface hydrology. Earth Planet. Sci. Lett. 266 (3), 332–344.

Biggs, J., Bastow, I.D., Keir, D., Lewi, E., 2011. Pulses of deformation reveal frequently recurring shallow magmatic activity beneath the Main Ethiopian Rift. Geochem. Geophys. Geosyst. 12.

Bilham, R., Bendick, R., Larson, K., Mohr, P., Braun, J., Tesfaye, S., Asfaw, L., 1999. Secular and tidal strain across the main Ethiopian rift. Geophys. Res. Lett. 26, 2789–2792.

Birhanu, Y., Bendick, R., 2015. Monsoonal loading in Ethiopia and Eritrea from vertical GPS displacement time series. J. Geophys. Res. Solid Earth 120 (10), 7231–7238.

Birhanu, Y., Bendick, R., Fisseha, S., Lewi, E., Floyd, M., King, R., Reilinger, R., 2016. GPS constraints on broad scale extension in the Ethiopian Highlands and Main Ethiopian Rift. Geophys. Res. Lett. 43 (13), 6844–6851.

Braddock, M., Biggs, J., Watson, I.M., Hutchison, W., Pyle, D.M., Mather, T.A., 2017. Satellite observations of fumarole activity at Aluto volcano, Ethiopia: implications for geothermal monitoring and volcanic hazard. J. Volcanol. Geotherm. Res. 341, 70–83.

Brisbourne, A., 2012. How to store and share geophysical data. Astron. Geophys. 53 (4), 19–20.

Christensen, N.I. (Ed.), 1984. Seismic Velocities. CRC Press, Boca Raton, Florida (228 pp.).

Christiansen, L., Hurwitz, S., Saar, M., Ingebritsen, S., Hsieh, P., 2005. Seasonal seismicity at western United States volcanic centers. Earth Planet. Sci. Lett. 240 (2), 307–321.

Christiansen, L., Hurwitz, S., Ingebritsen, S.E., 2007. Annual modulation of seismicity along the San Andreas Fault near Parkfield, CA. Geophys. Res. Lett. 34 (4).

Costain, J., Bollinger, G., 2010. Review: research results in hydroseismicity from 1987 to 2009. Bull. Seismol. Soc. Am. 100 (5A), 1841–1858.

Costain, J., Bollinger, G., Speer, J., 1987. Hydroseismicity—a hypothesis for the role of water in the generation of intraplate seismicity. Geology 15 (7), 618–621.

Daly, E., Keir, D., Ebinger, C., Stuart, G., Bastow, I., Ayele, A., 2008. Crustal tomographic imaging of a transitional continental rift: the Ethiopian rift. Geophys. J. Int. 172 (3), 1033–1048.

Darling, W.G., Gizaw, B., Arusei, M.K., 1996. Lake-groundwater relationships and fluid-rock interaction in the East African Rift Valley: isotopic evidence. J. Afr. Earth Sci. 22 (4), 423–431.

De Natale, G., Troise, C., Pingue, F., 2001. A mechanical fluid-dynamical model for ground movements at Campi Flegrei caldera. J. Geodyn. 32 (4–5), 487–517.

Ebmeier, S.K., Elliott, J.R., Nocquet, J.-M., Biggs, J., Mothes, P., Jarrín, P., Yépez, M., Aguaiza, S., Lundgren, P., Samsonov, S.V., 2016. Shallow earthquake inhibits unrest near Chiles–Cerro Negro volcanoes, Ecuador–Colombian border. Earth Planet. Sci. Lett. 450, 283–291.

Ellsworth, W.L., 2013. Injection-induced earthquakes. Science 341 (6142), 1225942.

Fialko, Y., Simons, M., 2000. Deformation and seismicity in the Coso geothermal area, Inyo County, California: observations and modeling using satellite radar interferometry. J. Geophys. Res. 105 (B9), 21781–21793.

Fu, Y., Argus, D.F., Landerer, F.W., 2015. GPS as an independent measurement to estimate terrestrial water storage variations in Washington and Oregon. J. Geophys. Res. Solid Earth 120 (1), 552–566.

Gardner, J., Knopoff, L., 1974. Is the sequence of earthquakes in Southern California, with aftershocks removed, Poissonian? Bull. Seismol. Soc. Am. 64 (5), 1363–1367.

Gaucher, E., Schoenball, M., Heidbach, O., Zang, A., Fokker, P.A., van Wees, J.-D., Kohl, T., 2015. Induced seismicity in geothermal reservoirs: a review of forecasting approaches. Renew. Sust. Energ. Rev. 52, 1473–1490.

Gianelli, G., Teklemariam, M., 1993. Water-rock interaction processes in the Aluto-Langano geothermal field (Ethiopia). J. Volcanol. Geotherm. Res. 56, 429–445.

Gizaw, B., 1993. Aluto-Langano geothermal field, Ethiopian rift valley: physical characteristics and the effects of gas on well performance. Geothermics 22 (2), 101–116.

Grünthal, G., 2014. Induced seismicity related to geothermal projects versus natural tectonic earthquakes and other types of induced seismic events in Central Europe. Geothermics 52, 22–35.

Hainzl, S., Kraft, T., Wassermann, J., Igel, H., Schmedes, E., 2006. Evidence for rainfall-triggered earthquake activity. Geophys. Res. Lett. 33 (19).

Harris, I., Jones, P., Osborn, T., Lister, D., 2014. Updated high-resolution grids of monthly climatic observations–the CRU TS3. 10 Dataset. Int. J. Climatol. 34 (3), 623–642.

Herring, T., King, R., McClusky, S., 2010. Introduction to Gamit/Globk. Massachusetts Institute of Technology, Cambridge, Massachusetts.

Hochstein, M.P., Oluma, B., Hole, H., 2017. Early exploration of the Aluto geothermal field, Ethiopia (History of discovery well LA-3). Geothermics 66, 73–84.

Hutchison, W., Mather, T.A., Pyle, D.M., Biggs, J., Yirgu, G., 2015. Structural controls on fluid pathways in an active rift system: a case study of the Aluto volcanic complex. Geosphere 11 (3), 542–562.

Hutchison, W., Pyle, D.M., Mather, T.A., Yirgu, G., Biggs, J., Cohen, B.E., Barfod, D.N., Lewi, E., 2016a. The eruptive history and magmatic evolution of Aluto volcano: new insights into silicic peralkaline volcanism in the Ethiopian rift. J. Volcanol. Geotherm. Res. 328, 9–33.

Hutchison, W., Biggs, J., Mather, T.A., Pyle, D.M., Lewi, E., Yirgu, G., Caliro, S., Chiodini, G., Clor, L.E., Fischer, T.P., 2016b. Causes of unrest at silicic calderas in the East African Rift: new constraints from InSAR and soil-gas chemistry at Aluto volcano, Ethiopia. Geochem. Geophys. Geosyst. 17 (8), 3008–3030.

Hutchison, W., Fusillo, R., Pyle, D.M., Mather, T.A., Blundy, J.D., Biggs, J., Yirgu, G., Cohen, B.E., Brooker, R.A., Barfod, D.N., 2016c. A pulse of mid-Pleistocene rift volcanism in Ethiopia at the dawn of modern humans. Nat. Commun. 7.

Jiménez, M.-J., García-Fernández, M., 2000. Occurrence of shallow earthquakes following periods of intense rainfall in Tenerife, Canary Islands. J. Volcanol. Geotherm. Res. 103 (1), 463–468.

Kebede, S., Mamo, T., Abebe, T., 1985. Explanation to the geological map of Aluto-Langano geothermal area. Tech. Rep. Ethiopian Institute of Geological Surveys Addis Ababa, Ethiopia.

Keir, D., Ebinger, C.J., Stuart, G.W., Daly, E., Ayele, A., 2006. Strain accommodation by magmatism and faulting as rifting proceeds to breakup: seismicity of the northern Ethiopian rift. J. Geophys. Res. Solid Earth 111, 5314.

Kogan, L., Fisseha, S., Bendick, R., Reilinger, R., McClusky, S., King, R., Solomon, T., 2012. Lithospheric strength and strain localization in continental extension from observations of the East African Rift. J. Geophys. Res. Solid Earth 117 (B3).

Landerer, F.W., Swenson, S., 2012. Accuracy of scaled GRACE terrestrial water storage estimates. Water Resour. Res. 48 (4).

Lee, M.K., Wolf, L.W., 1998. Analysis of fluid pressure propagation in heterogeneous rocks: implications for hydrologically-induced earthquakes. Geophys. Res. Lett. 25 (13), 2329–2332.

Lomax, A., Virieux, J., Volant, P., Berge-Thierry, C., 2000. Probabilistic earthquake location in 3D and layered models. Advances in Seismic Event Location. Springer, pp. 101–134.

Mazzarini, F., Keir, D., Isola, I., 2013. Spatial relationship between earthquakes and volcanic vents in the central-northern Main Ethiopian Rift. J. Volcanol. Geotherm. Res. 262, 123–133.

McClellan, P.H., 1984. Earthquake seasonality before the 1906 San Francisco earthquake. Nature 307 (5947), 153–156.

Mepham, R., Hughes, R., Hughes, J., 1992. A Directory of African Wetlands. IUCN, UNEP and WCMC, Cambridge.

Parker, A.L., Filmer, M.S., Featherstone, W.E., 2017. First results from Sentinel-1A InSAR over Australia: application to the Perth Basin. Remote Sens. 9 (3), 299.

Prejean, S., Hill, D., Brodsky, E., Hough, S., Johnston, M., Malone, S., Oppenheimer, D., Pitt, A., Richards-Dinger, K., 2004. Remotely triggered seismicity on the United States west coast following the Mw 7.9 Denali fault earthquake. Bull. Seismol. Soc. Am. 94 (6B), S348–S359.

Press, F., 1966. Section 9: seismic velocities. Geol. Soc. Am. Mem. 97, 195–218.

Pritchard, M., Jay, J., Aron, F., Henderson, S., Lara, L., 2013. Subsidence at southern Andes volcanoes induced by the 2010 Maule, Chile earthquake. Nat. Geosci. 6 (8), 632–636.

Reasenberg, P., 1985. Second-order moment of central California seismicity, 1969–1982. J. Geophys. Res. Solid Earth 90 (B7), 5479–5495.

Reilinger, R., McClusky, S., Vernant, P., Lawrence, S., Ergintav, S., Cakmak, R., Ozener, H., Kadirov, F., Guliev, I., Stepanyan, R., 2006. GPS constraints on continental deformation in the Africa-Arabia-Eurasia continental collision zone and implications for the dynamics of plate interactions. J. Geophys. Res. Solid Earth 111 (B5).

Saar, M.O., Manga, M., 2003. Seismicity induced by seasonal groundwater recharge at Mt. Hood, Oregon. Earth Planet. Sci. Lett. 214 (3), 605–618.

Samrock, F., Kuvshinov, A., Bakker, J., Jackson, A., Fisseha, S., 2015. 3-D analysis and interpretation of magnetotelluric data from the Aluto-Langano geothermal field, Ethiopia. Geophys. J. Int. 202 (3), 1923–1948.

Schuster, A., 1898. On the investigation of hidden periodicities with application to a supposed 26 day period of meteorological phenomena. Terr. Magn. 3 (1), 13–41.

Senbete, G., 2014. Baseline survey for "Sustainable development of the Gambella and Rift Valley Landscapes" project. Technical Report. Lake Ziway Fisheries and Water Resources Office, Ziway, Ethiopia.

Simpson, D., Leith, W., Scholz, C., 1988. Two types of reservoir-induced seismicity. Bull. Seismol. Soc. Am. 78 (6), 2025–2040.

Stewart, I.S., Sauber, J., Rose, J., 2000. Glacio-seismotectonics: ice sheets, crustal deformation and seismicity. Quat. Sci. Rev. 19 (14), 1367–1389.

Talwani, P., Chen, L., Gahalaut, K., 2007. Seismogenic permeability, ks. J. Geophys. Res. Solid Earth 112 (B7).

Teklemariam, M., Battaglia, S., Gianelli, G., Ruggieri, G., 1996. Hydrothermal alteration in the Aluto-Langano geothermal field, Ethiopia. Geothermics 25 (6), 679–702.

Uhrhammer, R., 1986. Characteristics of northern and central California seismicity. Earthq. Notes 57 (1), 21.

Vasco, D., Rucci, A., Ferretti, A., Novali, F., Bissell, R., Ringrose, P., Mathieson, A., Wright, I., 2010. Satellite-based measurements of surface deformation reveal fluid flow associated with the geological storage of carbon dioxide. Geophys. Res. Lett. 37 (3).

Vasco, D., Rutqvist, J., Ferretti, A., Rucci, A., Bellotti, F., Dobson, P., Oldenburg, C., Garcia, J., Walters, M., Hartline, C., 2013. Monitoring deformation at the Geysers Geothermal Field, California using C-band and X-band interferometric synthetic aperture radar. Geophys. Res. Lett. 40 (11), 2567–2572.

Verdon, J.P., 2014. Significance for secure CO2 storage of earthquakes induced by fluid injection. Environ. Res. Lett. 9 (6), 064022.

Wahr, J., Khan, S.A., Dam, T., Liu, L., Angelen, J.H., Broeke, M.R., Meertens, C.M., 2013. The use of GPS horizontals for loading studies, with applications to northern California and southeast Greenland. J. Geophys. Res. Solid Earth 118 (4), 1795–1806.

Wilks, M., Kendall, J.-M., Nowacki, A., Biggs, J., Wookey, J., Birhanu, Y., Ayele, A., Bedada, T., 2017. Seismicity associated with magmatism, faulting and hydrothermal circulation at Aluto Volcano, Main Ethiopian Rift. J. Volcanol. Geotherm. Res. 340, 52–67.

Wolf, L.W., Rowe, C.A., Horner, R.B., 1997. Periodic seismicity near Mt. Ogden on the Alaska-British Columbia border: a case for hydrologically triggered earthquakes? Bull. Seismol. Soc. Am. 87 (6), 1473–1483.